Supplementary Information for

Single-molecule fluorescence imaging and deep learning reveal highly heterogeneous aggregation of amyloid-β 42

Fanjie Meng*, Janghyun Yoo*, and Hoi Sung Chung*

*e-mail:
fanjie.meng@nih.gov (F.M.); janghyun.yoo@nih.gov (J.Y.); chunghoi@niddk.nih.gov (H.S.C)

This PDF file includes:

Supplementary Text
Figures S1 - S12
Legends for Movies S1 – S18
SI References

Other supplementary materials for this manuscript include the following:

Movies S1 – S18

SI Text

Materials and Methods

Protein expression

The amino acid and DNA sequences of Aβ42 are shown in Fig. S1. For labeling of fluorescence dyes, a cysteine residue was attached to the N- terminal of Aβ42 (Avi-C-Aβ42 and C-Aβ42). To check the growth of fibrils from immobilized proteins on a biotin-embedded glass coverslip, a biotin accepting sequence (AviTag, Avidity LLC, Aurora, Colorado) and a flexible linker sequence were attached to the N-terminus of Aβ (Avi-C-Aβ42). All plasmids were constructed by DNA2.0 (DNA2.0, Neward, CA). To ensure the expression of biotinylated proteins, we co-expressed the BirA gene to generate sufficient biotin ligase (Avidity LLC).

We co-transformed *E. coli* strain BL-21 (DE3) (Stratagene, La Jolla, CO) with kanamycin-resistant pJ411-BirA, and carbenicillin-resistant pJ414-Aβ, for the expression of Avi-C-Aβ42. For Aβ42 and C-Aβ42, we transformed the bacteria with pJ414-Aβ. The expression level of the full-length protein was optimized by varying the ratio of the plasmids. The optimized condition was 0.2 μL of pJ411-BirA (50 ng/μL) and 0.2 μL of a protein construct (20 ng/μL). Co-transformed bacteria were spread on LB-agar plates with corresponding antibiotics. After incubation at 37°C overnight, 2 - 3 individual colonies were picked and inoculated in 5 mL LB broth with the same antibiotics combinations for 16 - 24 hours at 37°C with shaking at 250 rpm. Colonies grown up in liquid medium were diluted into the same medium of 500 - 1000 mL for further growth. After incubation for 3 - 5 hours, expression was induced at OD 0.6 (600 nm) with final concentrations of 1 mM IPTG, and 50 μM *d*-biotin. After overnight incubation at 25°C with shaking at 250 rpm, bacteria was harvested and spun down at 8000 g for 10 minutes using Sorvall LYNX 4000 centrifuge (Thermo Scientific, Waltham, MA). After removing the supernatant, pellets were either used for lysis right away or frozen at - 20°C for future use.

Purification of proteins

Bacteria pellets from 500 mL LB culture were lysed in 20 mL of bacterial protein extraction reagent (B-Per, Thermo Fisher Scientific, Grand Island, NY) with 50 mM benzamidine hydrochloride, 100 μg/mL lysozyme (Sigma, St. Louis, MO), and 5 units of benzonase (Novogen, Madison, WI). The pellets were mixed and resuspended in the lysis buffer and incubated at room temperature for 30 minutes. The lysate was transferred to 50 mL spinning tubes and centrifuged at 30000 g for 45 minutes with Sorvall LYNX 4000. The supernatant was removed for electrophoresis and the pellet containing inclusion bodies were resuspended in 30 mL 1× PBS solution with 10 mM DTT and 1% Triton X-100 and sonicated three times for 20 seconds on ice using a sonicator at 100% power (Model Q55, Qsonica, Newtown, CT). The solution was then centrifuged at 30000 g for 30 minutes at 4°C. The supernatant was discarded and the remaining pellet was resuspended in the same PBS buffer used in the previous sonication step. One molar sodium chloride was added to remove DNA and RNA from pellets. The mixture was sonicated as in the previous step and centrifuged at 30000 g for 30 minutes at 4°C. Resuspension, sonication, and centrifugation were repeated in 1× PBS. The pellet containing inclusion bodies was dissolved in 5 mL of 50 mM Tris-HCl with 6 M guanidine hydrochloride (GdmCl) and 10 mM DTT and kept at room temperature overnight for complete extraction of Aβ proteins. The solution was then centrifuged at 30000 g at 4°C for 45 minutes to remove the insoluble pellet. The supernatant was collected for further purification. The supernatant was loaded on PhastSystem (Pharmacia, Baltimore, MD) gels. Gels were stained with Phastgel Blue

R (Pharmacia, Baltimore, MD) then washed until protein bands were clearly shown. Aβ proteins with and without AviTag and linker appeared at 8 kDa and 5 kDa on gels, respectively, and these were the smallest proteins presenting in the inclusion body. The protein solutions (200 μL) were loaded onto the AKTA pure FPLC system equipped with a Superdex^{TM}75 10/300GL size exclusion column (GE Healthcare, Chicago, IL). The separation was run with 50 mM Tris-HCl, 4 M GdmCl solution at a flow rate of 0.8 mL/min. The fractions containing 5 kDa or 8 kDa proteins identified by Phastgel were collected and concentrated using Amicon Ultra centrifugal filters (EMD Millipore, Billerica, MA) and then subjected to the second round of FPLC purification.

Dye-labeling and purification

We labeled Avi-C-Aβ42 with Alexa Fluor 488 maleimide (Alexa 488, A10254, Thermo Fisher Scientific, Carlsbad, CA) and C-Aβ42 with Alexa Fluor 594 maleimide (Alexa 594, A10256, Thermo Fisher Scientific, Carlsbad, CA). Aβ (~ 0.2 mg) in 4 M GdmCl Tris buffer solution (pH 8) was concentrated to 100 μL in 6 M GdmCl using Amicon centrifugal filters and pH was adjusted to 7.0 by acetate buffer. 100 μL of protein solution was mixed with 0.1 mg of Alexa 488 or 594 pre-dissolved in 5 μL of DMSO. We incubated the mixture at room temperature overnight. Then the reaction was quenched by adding 4 μL of β-mercaptoethanol. The reaction mixture was fractionated on a Superdex^{TM}75 10/300GL size exclusion column equilibrated with 50 mM Tris-HCl, pH 8.0, 4 M GdmCl to remove the excess free dye. The peptide labeled with the dyes showed overlapping peaks of absorbance monitored at 280, 494 nm for Alexa 488, and 280, 594 nm for Alexa 594. The labeled protein concentration was determined by the absorbance at 494 nm or 594 nm measured by Cary 8454 UV-Vis spectrophotometer (Agilent Technologies, Santa Clara, CA). Purified samples were aliquoted into 10 μL and kept at - 80°C for future experiments.

Plate reader experiment for monitoring Aβ aggregation

A protein sample (20 - 50 μL) was loaded into 96-well half-bottom none binding surface polystyrene plates (REF 3881, Corning, Kennebunk, ME) for plate reader recording (Spark, TECAN, Switzerland). To monitor the aggregation of unlabeled Aβ42, Aβ42 stock solution (30 μM) was diluted into 6 μM thioflavin T (ThT, Sigma, St. Louis, MO) in 1× PBS (pH 7.4) to the final concentration of 2 μM and volume of 50 μL. All wells were sealed with a piece of parafilm to prevent evaporation in the bottom reading mode. The aggregation was monitored at 37ºC for several hours. The fluorescence signal was recorded every 5 min. Samples were excited (50 flashes) at 420 nm (ThT) and 575 nm (Alexa 594) and fluorescence was detected at 480 nm (ThT) and 627 nm (Alexa 594) with a 20 nm bandwidth. The focus along *z*-axis was set manually at 29500 μm and the automatic gain regulation feature was used.

Electron microscopy experiment

The fibrils of unlabeled Aβ42 and Alexa 594-Aβ42, prepared by incubating 5 μM proteins at 37ºC overnight, were imaged with FEI Morgagni microscope, which was operated at 80 kV and equipped with an AMT Advantage HR CCD camera. The samples were adsorbed to glow-discharged carbon films on lacey-carbon-coated copper mesh grids for 1 min, rinsed with deionized water, stained with 3% uranyl acetate for 1 min, and dried in air for imaging.

Fluorescence lifetime imaging (FLIM)

Single-molecule fluorescence imaging experiment was performed using a confocal microscope system (MicroTime200, Picoquant) with a 75 μm diam. pinhole, a beamsplitter (Z488/594rpc,

Chroma Technology), and an oil-immersion objective (UPLSAPO, NA 1.4, × 100, Olympus) (1). The sample was excited by a 485 nm diode laser (LDH-D-C-485, PicoQuant). Alexa 488 and Alexa 594 fluorescence was split into two channels using a beamsplitter (585DCXR, Chroma Technology) and focused through optical filters (ET525/50m for Alexa 488, E600LP for Alexa 594, Chroma Technology) onto photon-counting avalanche photodiodes (SPCM-AQR-16, PerkinElmer Optoelectronics).

We immobilized Alexa 488-labeled Avi-D-Aβ42 on a biotin-embedded, polyethyleneglycol-coated glass coverslip (Bio_01, Microsurfaces Inc.) via a biotin (surface)-NeutrAvidin-biotin (protein) linkage (2) and incubated with 500 nM of A-Aβ42 in 1× PBS, pH 7.5, including a cocktail of 100 mM β-mercaptoethanol, 10 mM Cystamine (3), 2 mM 4-nitrobenzyl alcohol (NBA), 2 mM cyclooctatetraene (COT), and 2 mM Trolox (4, 5) to reduce photoblinking and photobleaching of dyes. The purpose of this approach was to search for stepwise oligomer formation or fibril growth from immobilized donor-labeled Aβ42 monomer, but this was not observed. This finding is expected because the number of immobilized molecules is so much smaller than the number in solution, so the chance of stable oligomer formation originating from immobilized monomers is extremely low. Therefore, detected oligomers and fibrils contain only acceptor fluorophores (Alexa 594), which emit fluorescence after direct excitation (no energy transfer from Alexa 488) at the excitation wavelength, 485 nm. In FLIM experiments, a region of 10 × 10 μm^2 was raster scanned in the pulsed mode of the laser at 0.2 μW. The scan was repeated for 16 (4 × 4) – 36 regions (6 × 6). After finishing one round of scans (24 – 54 min), the stage was moved back to the first region and the scan was repeated, which results in movies of each region of 14 – 24 hours.

Since each region was scanned multiple times over a period of many hours, there were lateral drifts and defocusing. As seen in the movies, frame-by-frame movements of fibrils by several pixels were observed, which can result from both lateral drifts and actual movement on the surface. There was no experimental correction for these lateral movements. However, training of FNet was performed using the movies of overlapping fibrils synthesized by random samplings of the manually separable fibrils (i.e., non-overlapping fibrils) extracted from the experimental data. Therefore, the effect of lateral movements of fibrils are accounted for by the neural network model. Defocusing is more serious problem because it makes the image dimmer and blurry. To avoid this problem, the stage was re-focused along the axial direction prior to each raster scan.

Fig. S1. Amino acid and DNA sequences of Aβ42 constructs. (*A*) Amino acid sequence. A cysteine residue (magenta C) is appended to the N-terminus for C-Aβ42 and Avi-C-Aβ42. Biotin is attached to the lysine residue (blue K) in the AviTag sequence in the Avi-C-Aβ42 construct, which is separated from Aβ42 sequence by a flexible linker. (*B*) DNA sequences.

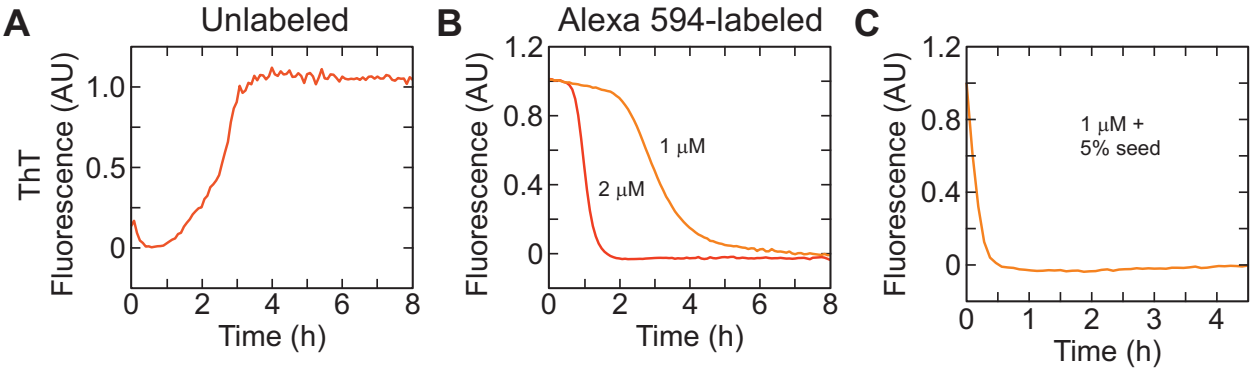

Fig. S2. Aggregation of Aβ42. (*A*) Aggregation of unlabeled Aβ42 (2 μM) at 37ºC monitored by Thioflavin T (ThT) fluorescence. (*B*) Aggregation of 1 and 2 μM of Alexa 594-labeled Aβ42 at 37ºC. (*C*) 5% addition of sonicated aggregate of Alexa 594-labeled Aβ42 eliminated the lag phase prior to aggregation (37ºC).

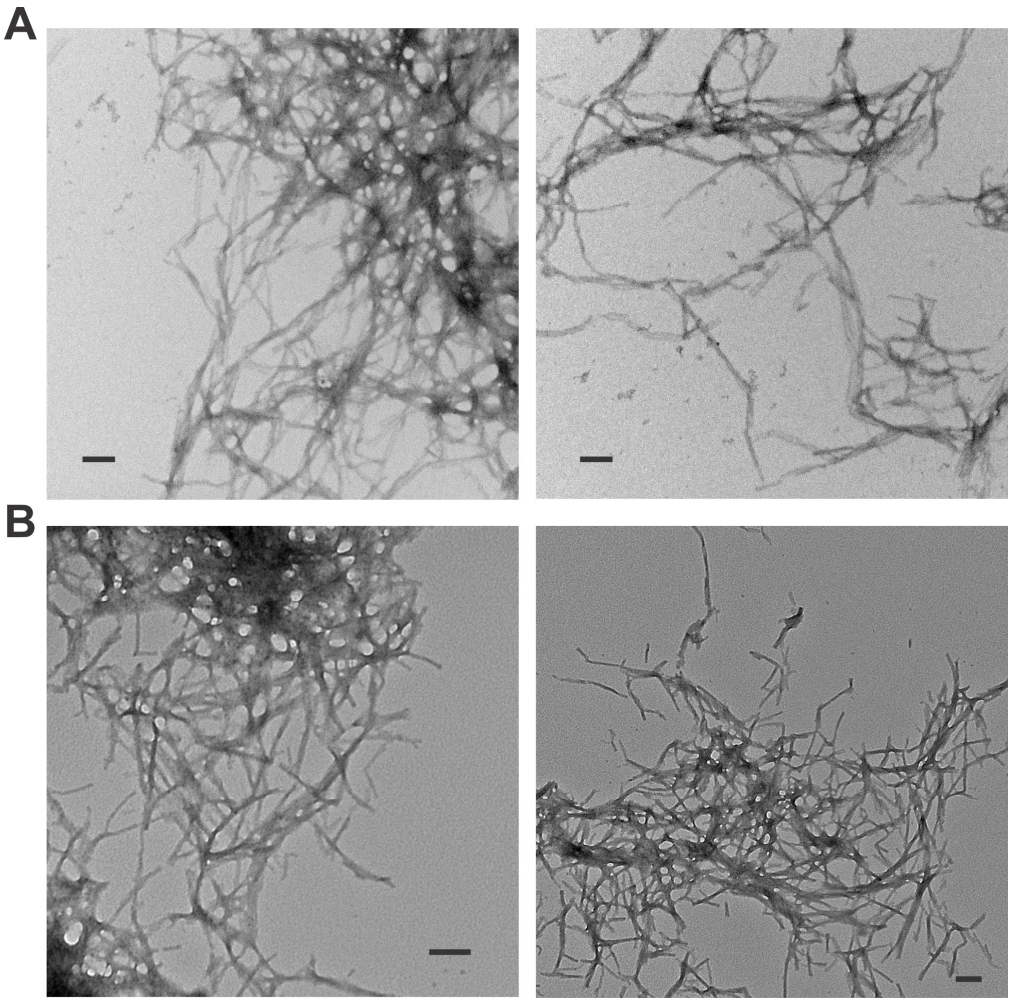

Fig. S3. Electron microscope images of fibrils. (*A*) Fibrils formed from 5 μM unlabeled Aβ42 at 37ºC overnight. (*B*) Fibrils formed from 5 μM Alexa 594-labeled Aβ42 at 37ºC overnight. Scale bars, 100 nm.

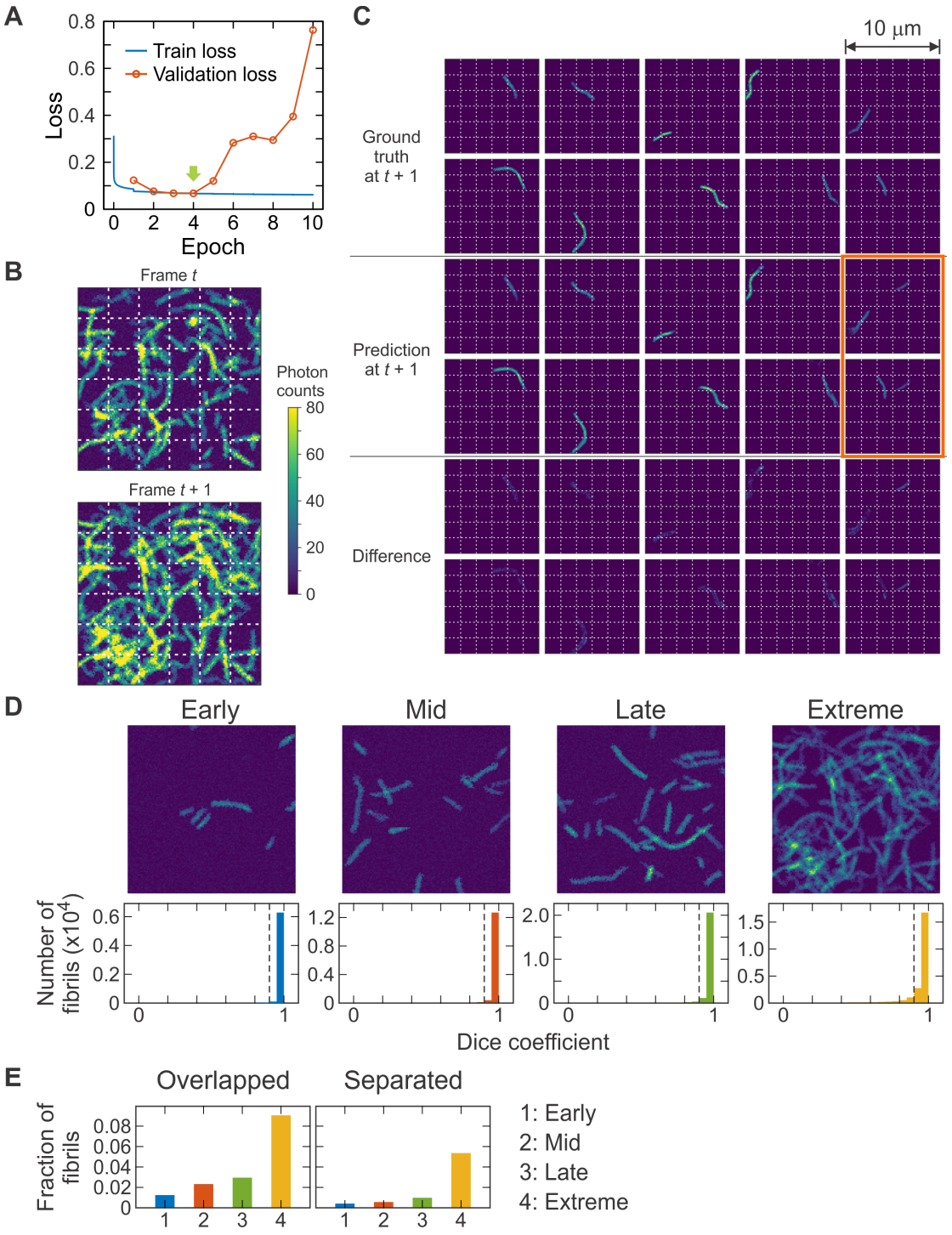

Fig. S4. Performance of FNet. (*A*) Validation of training. The model after epoch 4 with the lowest validation loss was used for the segmentation of experimental data. (*B*) Simulation of extremely highly overlapping fibril images (10 × 10 μm^2) at time *t* and *t* + 1. The density (126 fibrils per image) and growth speed (× 10) of fibrils in these images are much higher than those of typical experimental data. (*C*) Segmentation of the image at *t* + 1. Ground truth images (upper) and FNet predictions (middle) are compared. Fibrils inside the orange rectangle are misprediction. White grids are drawn in (B) and (C) to guide the locations of fibrils. (*D*) Dice coefficients (1 – *L* in Eq. (1)) calculated for the segmented fibrils in the simulations mimicking the early, mid and late phase of aggregation and an extreme case. An example image shows the fibril density in each case. Vertical dashed line at 0.9 is the criterion for the mis-segmentation in (E). (*E*) Fractions of mispredicted fibrils. (Left) Detection of more than one fibril overlapped. (Right) Detection of more than one fibril separated (fibrils inside orange box in (C)).

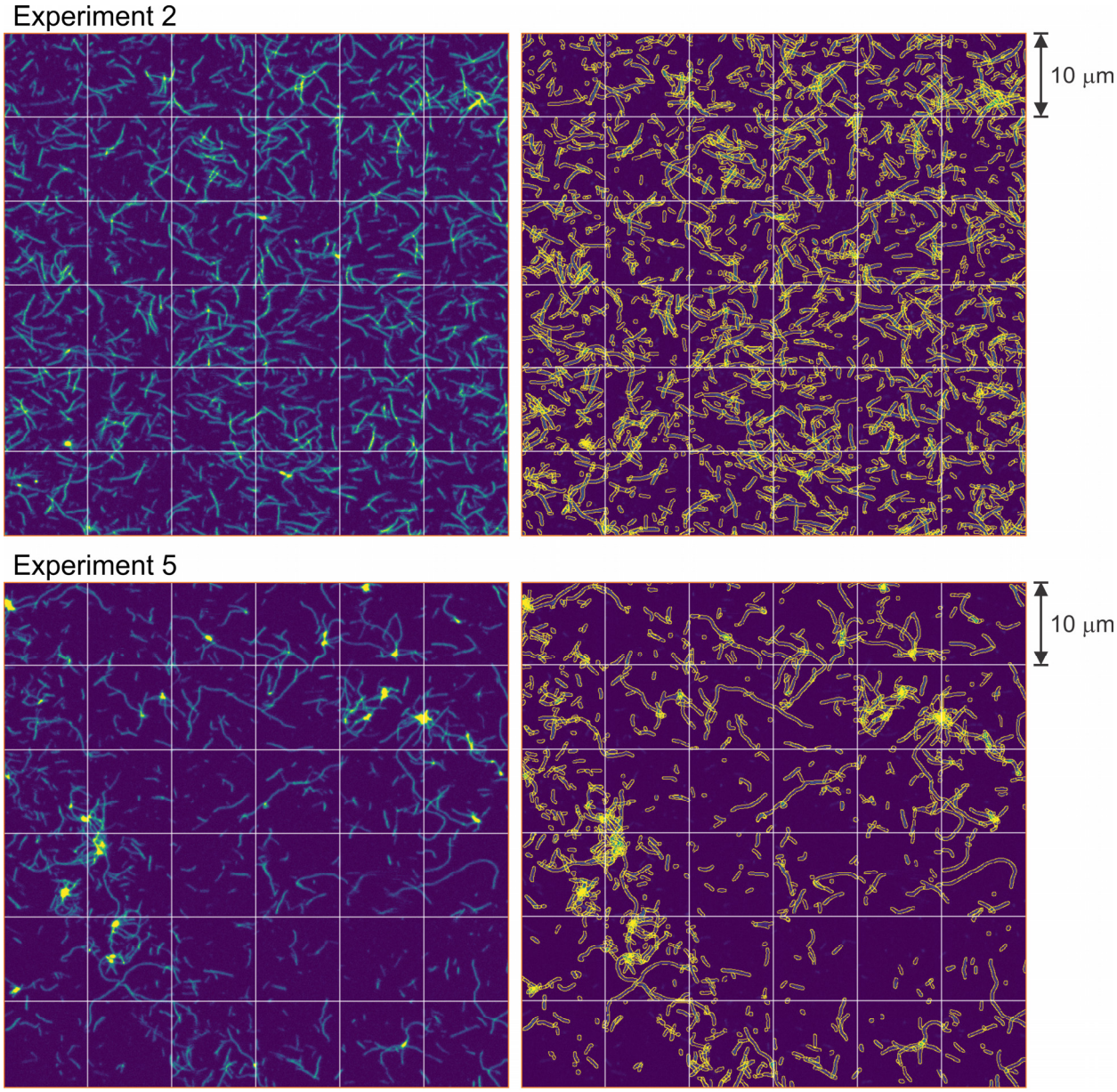

Fig. S5. Stitching of fibrils in adjacent image regions. (Left) The 6 × 6 scanned images are the last frames of experiment 2 (upper, 23 hours) and 5 (lower, 14 hours). (Right) Fibrils were segmented using FNet and the fibrils touching the boundaries of 10 × 10 μm^2 areas were merged with the continuing fibrils in the adjacent areas. Peripheries of individual fibrils are indicated by yellow contours.

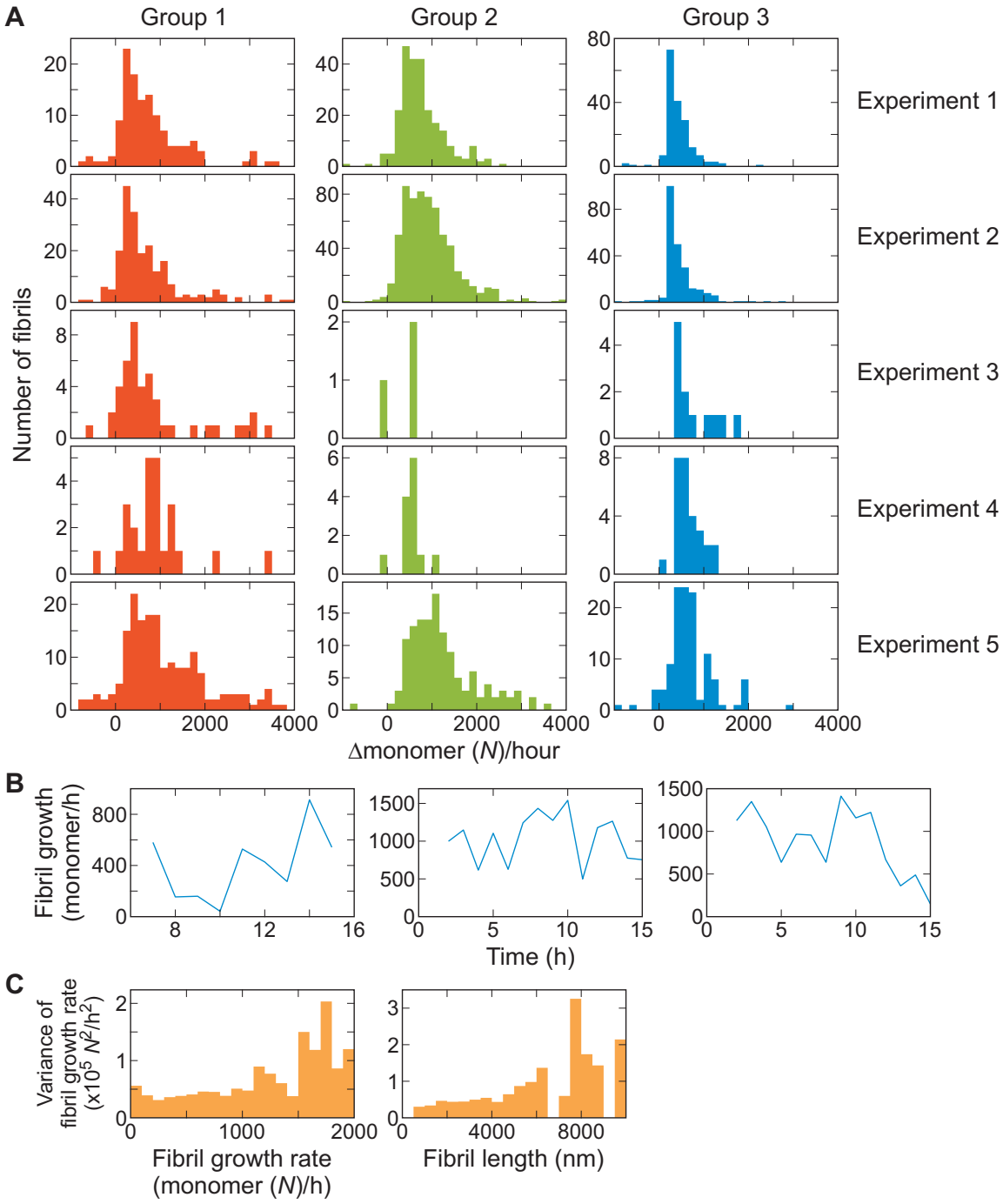

Fig. S6. Fibril growth analysis. (*A*) Growth rate of long fibrils of the three fibril groups in individual experiments. (*B*) Examples of the large fluctuation of the growth rate of three individual fibrils. (*C*) Dependence of the mean variance of the growth rate on the fibril growth rate (left) and fibril length (right). The variance of each growth rate trajectory was calculated as $\langle r^2 \rangle - \langle r \rangle^2$, where r is the growth rate at each time point in (B). The values for the fibrils with the lowest growth rate or shortest fibrils serve as the upper bound of the mean variance. Much larger variance of fast-growing or long fibrils than this upper bound indicates large fluctuations of the growth rate prevail.

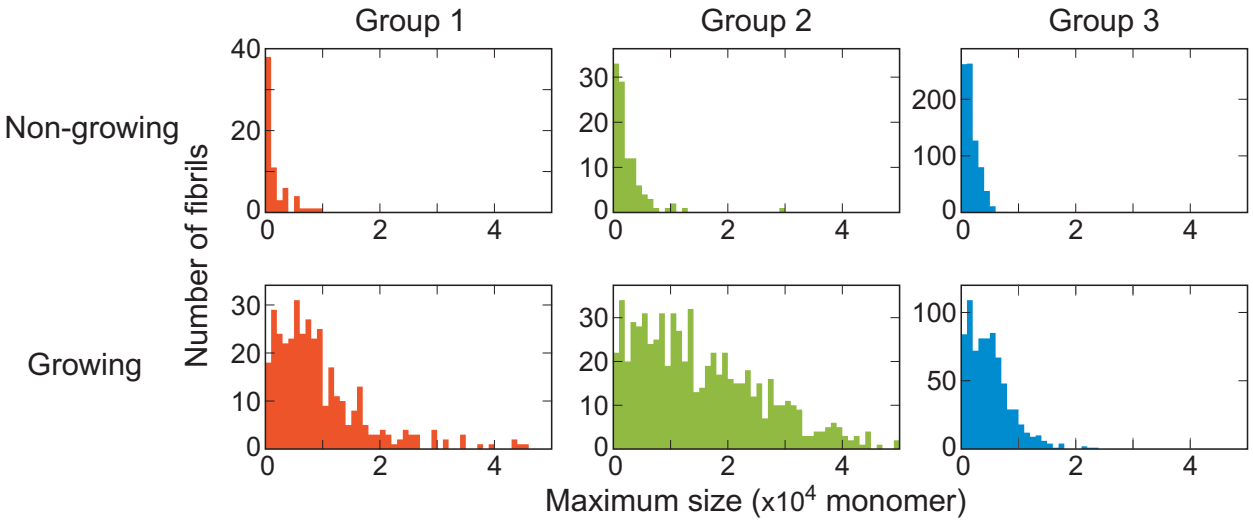

Fig. S7. Distribution of the maximum size of fibrils. The maximum size observed for each individual non-growing (upper) and growing (lower) fibrils of the three fibril groups.

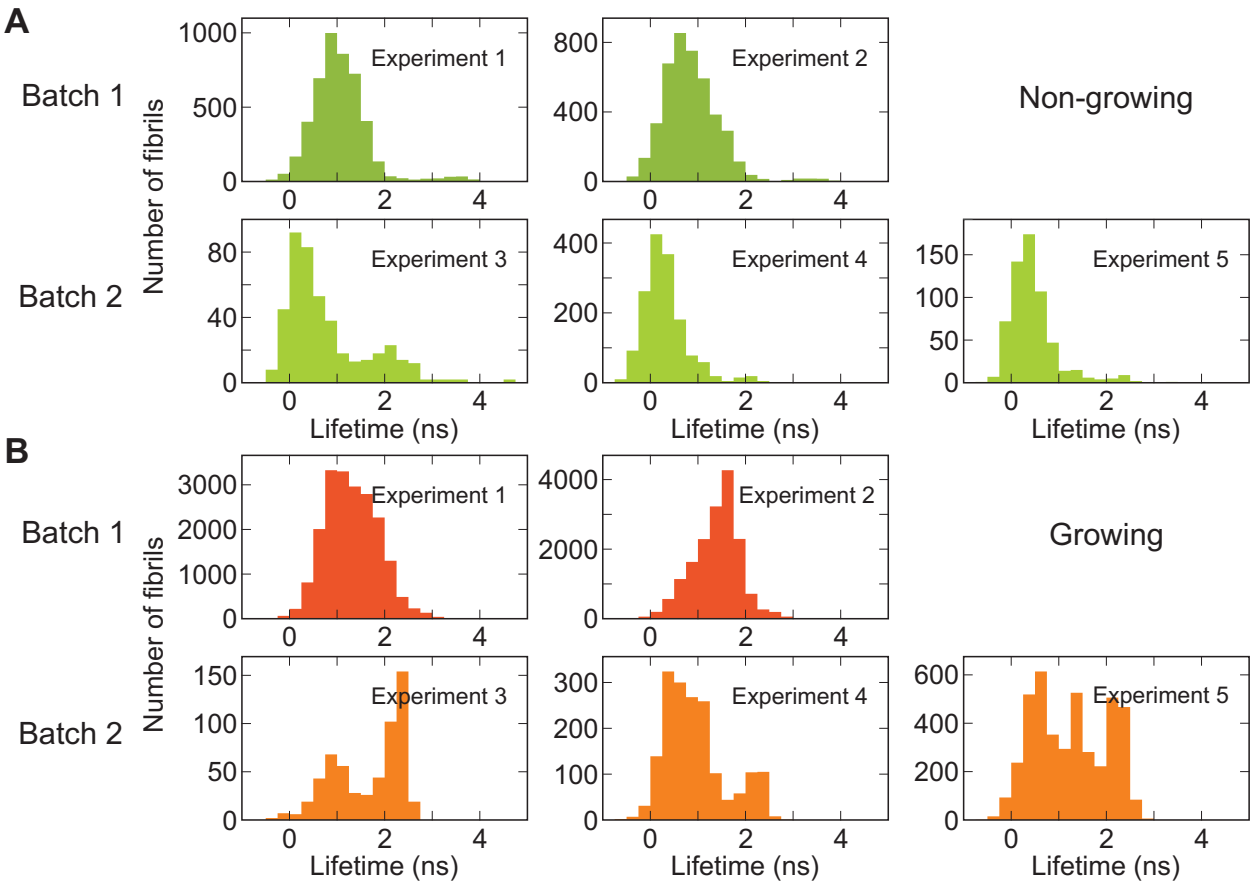

Fig. S8. Fluorescence lifetime distributions of fibrils from five individual experiments. (*A*) Non-growing fibrils. (*B*) Growing fibrils.

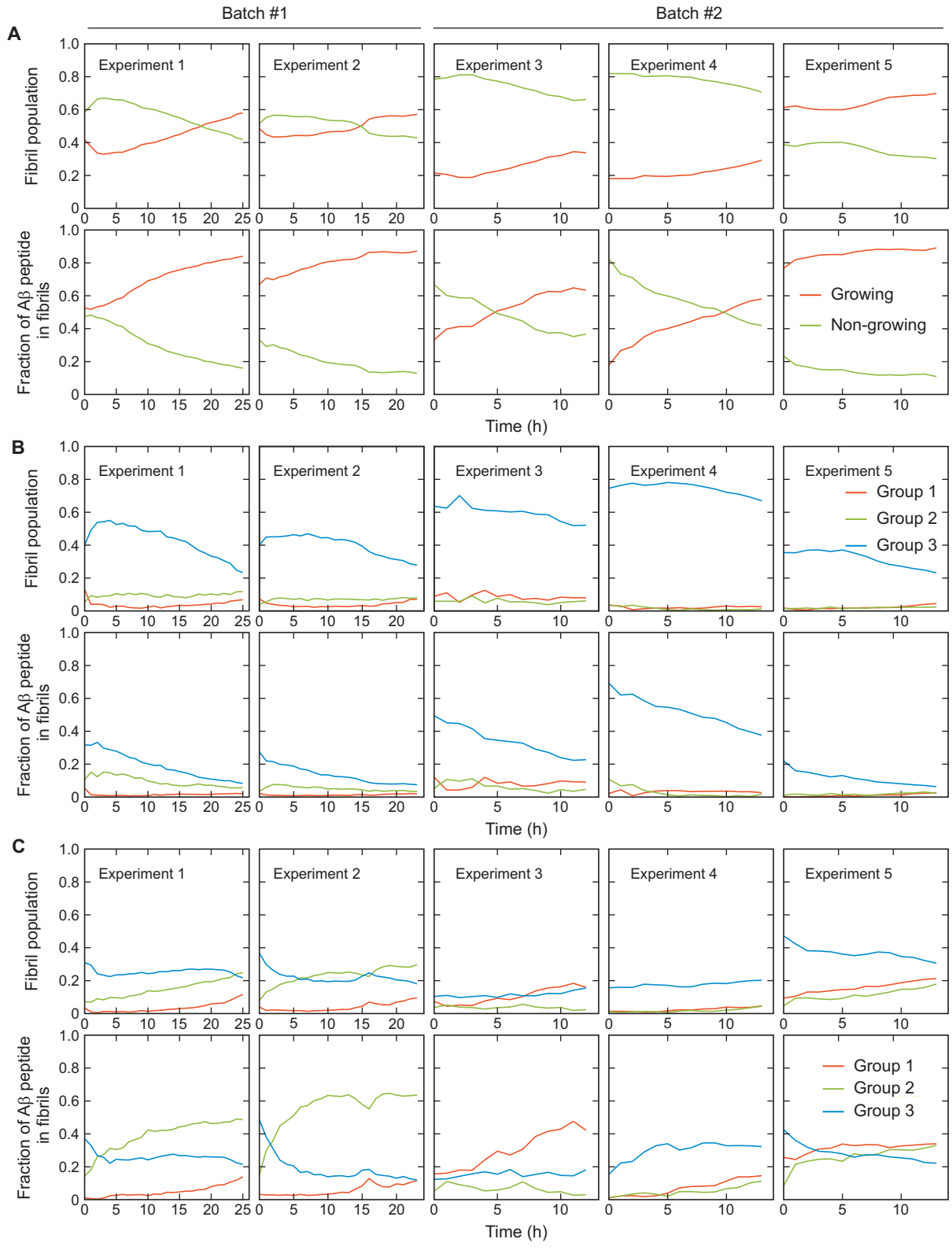

Fig. S9. Time-dependent changes of the fractions of monomers in various groups of fibrils from five different experiments. Upper panels show the fraction of number of fibrils and lower panels show fraction of Aβ peptide incorporated in fibrils of each category. (*A*) Non-growing (green) and growing (red) fibrils. (*B*) Three fibril groups of non-growing fibrils. (*C*) Three fibril groups of growing fibrils. (*B*, *C*) The fractions were normalized to the total number of fibrils (growing + non-growing) at each time point.

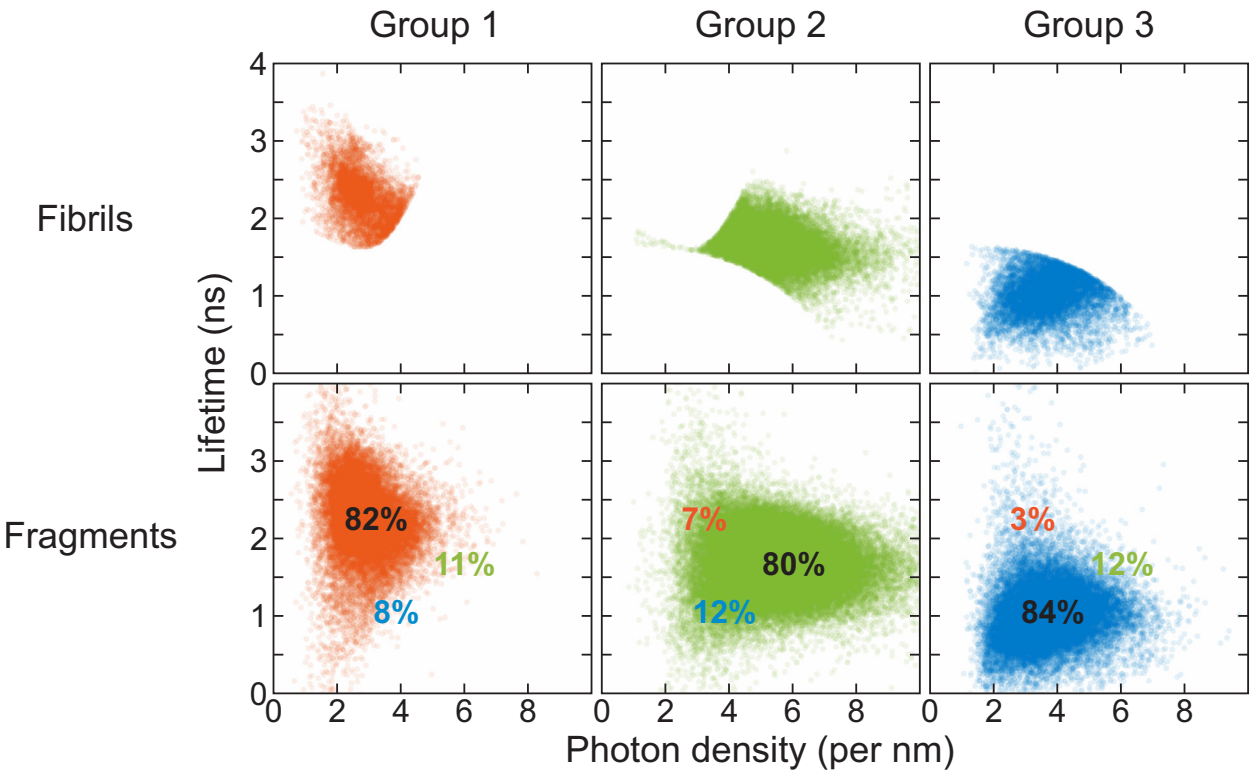

Fig. S10. Homogeneity of fibrils. 2D fluorescence lifetime and photon density plots of individual fibrils in the three fibril groups (Upper) and fragments in those fibrils (Lower). Most fragments belong to the same group of fibrils (80 – 84%) despite the broader distributions due to the smaller number of photons especially from the fibrils near the group boundaries, indicating individual fibrils are predominantly homogeneous. The fractions of the fragments penetrating into other groups are indicated by the percentages in corresponding colors.

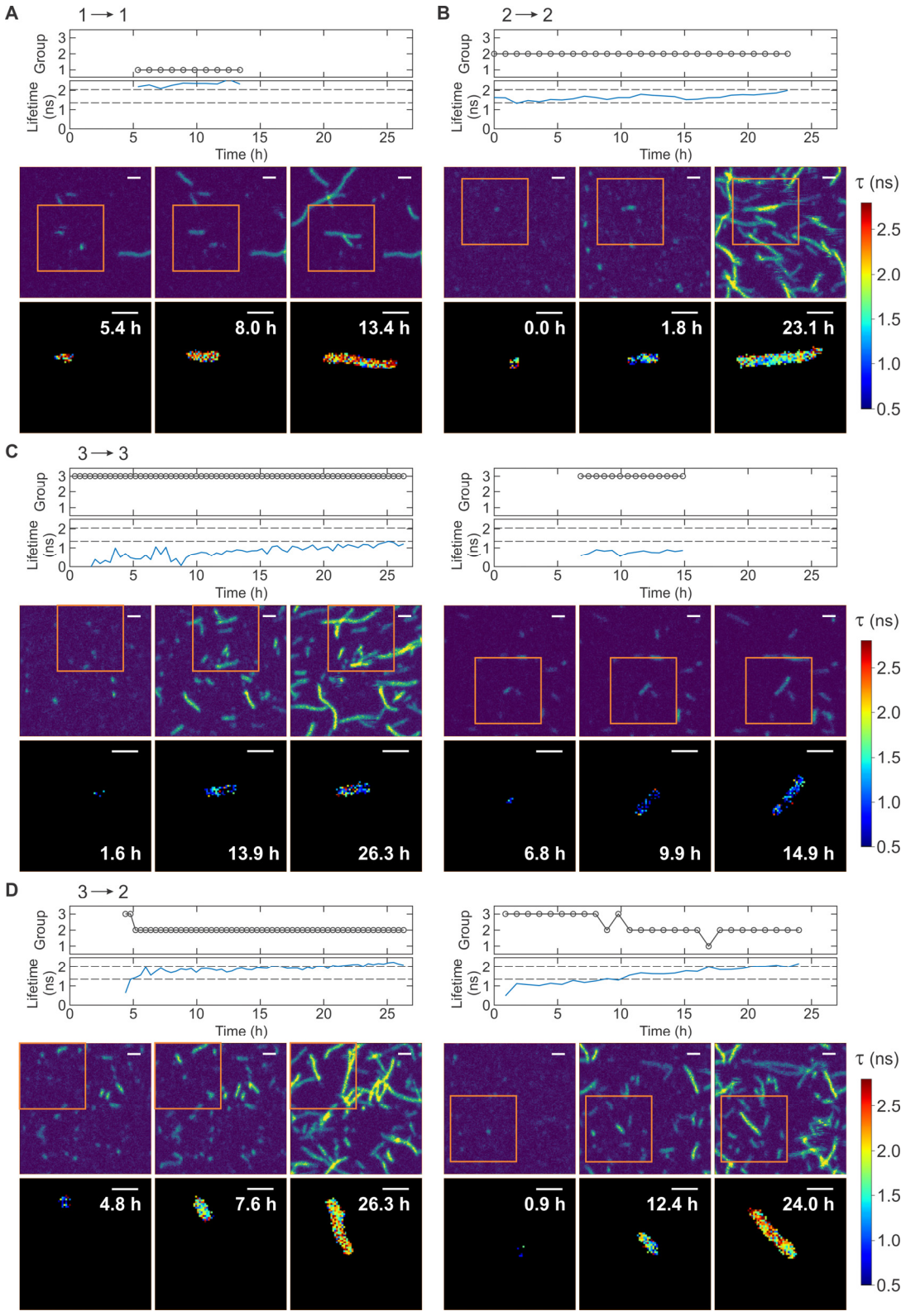

Fig. S11. Homogeneous and heterogeneous fibril growth. Time-dependent changes of the fibril groups and fluorescence lifetimes and snapshots of the fibril images are shown (*A* – *C*) for the fibrils grow homogeneously without changing groups (*A*) group 1 → 1, (*B*) 2 → 2, and (*C*) 3 → 3, and (*D*) for those exhibiting heterogeneous secondary nucleation (group 3 → 2, Movie S11 and S12). See Fig. 5 legend for the details of the group and lifetime trajectories and fibril images.

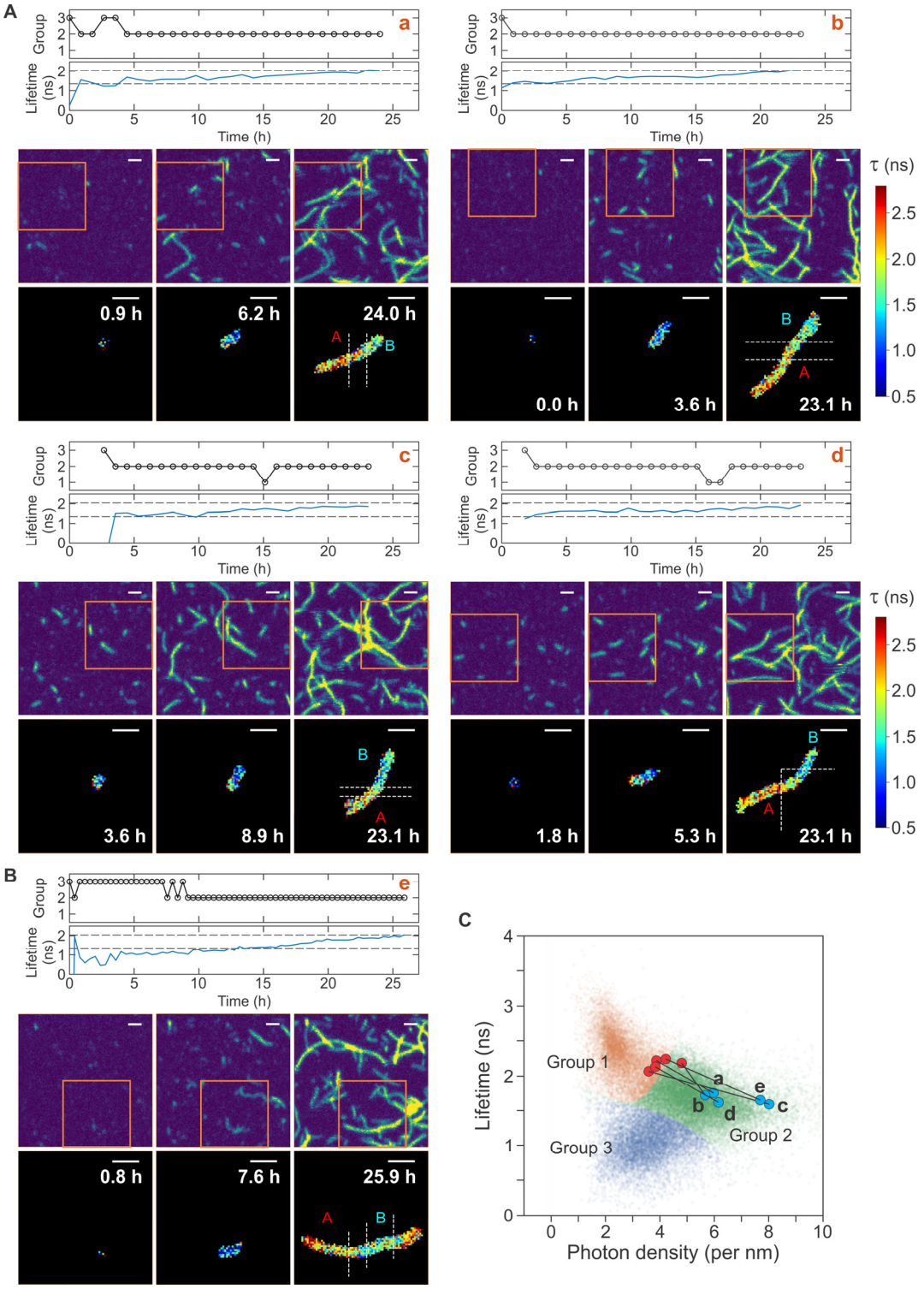

Fig. S12. Double heterogeneous secondary nucleation. Time-dependent changes of the fibril groups and fluorescence lifetimes and snapshots of the fibril images are shown for the fibrils growing both directions with group characteristics different from those of the oligomer origins. (*A*) The growth begins from a group 3 oligomer and ends with group 1 on one side and group 2 on the other side. (*B*) The growth begins from a group 3 oligomer and the middle part becomes group 2 while both ends grow as group 1. (*C*) 2D fluorescence lifetime and photon density plots of the two fragments (red dot: red A region; blue dot: cyan B region) of the five fibrils in (*A*) and (*B*) indicated by lower case letters (a – e, Movies S14 – S18). See Fig. 5 legend for the details of the group and lifetime trajectories and fibril images.

Movie Legends

Movie S1 (separate file). Fibril growth movie 1

Movie S2 (separate file). Fibril growth movie 2

Movie S3 (separate file). Fibril growth movie 3

Movie S4 (separate file). Fibril growth and segmentation movie, experiment 1

Movie S5 (separate file). Fibril growth and segmentation movie, experiment 2

Movie S6 (separate file). Fibril growth and segmentation movie, experiment 3

Movie S7 (separate file). Fibril growth and segmentation movie, experiment 4

Movie S8 (separate file). Fibril growth and segmentation movie, experiment 5

Movie S9 (separate file). Heterogeneous secondary nucleation in Fig. 5C (left)

Movie S10 (separate file). Heterogeneous secondary nucleation in Fig. 5C (right)

Movie S11 (separate file). Heterogeneous secondary nucleation in Fig. S11D (left)

Movie S12 (separate file). Heterogeneous secondary nucleation in Fig. S11D (right)

Movie S13 (separate file). Double heterogeneous secondary nucleation in Fig. 5D

Movie S14 (separate file). Double heterogeneous secondary nucleation in Fig. S12A (a)

Movie S15 (separate file). Double heterogeneous secondary nucleation in Fig. S12A (b)

Movie S16 (separate file). Double heterogeneous secondary nucleation in Fig. S12A (c)

Movie S17 (separate file). Double heterogeneous secondary nucleation in Fig. S12A (d)

Movie S18 (separate file). Double heterogeneous secondary nucleation in Fig. S12B (e)

SI References

1. Chung HS, et al. (2017) Oligomerization of the tetramerization domain of p53 probed by two- and three-color single-molecule FRET. *Proc Natl Acad Sci U S A* 114(33):E6812–E6821.
2. Chung HS, Louis JM, Eaton WA (2009) Experimental determination of upper bound for transition path times in protein folding from single-molecule photon-by-photon trajectories. *Proc Natl Acad Sci U S A* 106(29):11837–11844.
3. Nettels D, et al. (2009) Single-molecule spectroscopy of the temperature-induced collapse of unfolded proteins. *Proc Natl Acad Sci U S A* 106(49):20740–20745.
4. Zheng Q, Jockusch S, Zhou Z, Blanchard SC (2014) The contribution of reactive oxygen species to the photobleaching of organic fluorophores. *Photochem Photobiol* 90(2):448–454.
5. Zheng Q, et al. (2014) Ultra-stable organic fluorophores for single-molecule research. *Chem Soc Rev* 43(4):1044–1056.